ISSN 0016-7932, Geomagnetism and Aeronomy, 2006, Vol. 46, No. 3, pp. 275–293. © Pleiades Publishing, Inc., 2006.
Original Russian Text © K.G. Ivanov, E.P. Romashets, A.F. Kharshiladze, 2006, published in Geomagnetizm i Aeronomiya, 2006, Vol. 46, No. 3, pp. 291–309.

Solar–Terrestrial Storm of November 18–20, 2003. 1. Near-Earth Disturbances in the Solar Wind

K. G. Ivanov, E. P. Romashets, and A. F. Kharshiladze

Pushkov Institute of Terrestrial Magnetism, Ionosphere, and Radiowave Propagation, Russian Academy of Sciences, Troitsk, Moscow oblast, 142190 Russia

e-mail: kivanov@izmiran.troitsk.ru

Received July 20, 2005

Abstract—The structure, configuration, dynamics, and solar sources of the near-Earth MHD disturbance of the solar wind on November 20, 2003, is considered. The disturbances of October 24 and November 22 after flares from the same AR 10484 (10501) are compared. The velocity field in the leading part of the sporadic disturbance is for the first time studied in the coordinate system stationary relative to the bow shock. A possible scenario of the physical processes in the course of this solar–terrestrial storm is discussed in comparison with the previously developed scenario for the storm of July 15, 2000. It has been indicated that (1) the near-Earth disturbance was observed at the sector boundary (HCS) and in its vicinities and (2) the disturbance MHD structure included: the complicated bow shock, wide boundary layer with reconnecting fields at a transition from the shock to the magnetic cloud, magnetic cloud with a magnetic cavity including packed substance of an active filament, and return shock layer (supposedly). It has been found out that the shock front configuration and the velocity field are reproduced at an identical position of AR and HCS relative to the Earth on November 20 and 24. It has been indicated that the maximal magnetic induction in the cloud satisfied the condition $B_m = (8\pi n_1 m_p)^{1/2}(D - \mathbf{NV}_1)$, i.e., depended on the dynamic impact on the cloud during all three storms [Ivanov et al., 1974]. When the disturbance was related to solar sources, the attention has been paid to the parallelism of the axes of symmetry of the active filament, transient coronal hole, coronal mass ejection, zero line of the open coronal field (HCS), and the axis of the near-Earth magnetic cloud: the regularity previously established in the scenario of the storm of July 15, 2000 [Ivanov et al., 2005]. It has been indicated that the extremely large B_m value in the cloud of October 20 was caused by a strong suppression of the series of postflare shocks reflected from the heliospheric streamer.

PACS numbers: 94.30.Lr, 94.30.Va

DOI: 10.1134/S0016793206030017

1. INTRODUCTION

The main data on the storm of November 18–23, 2003, have been published in [Yermolaev et al., 2005]. Specifically, this work describes the interplanetary shock and magnetic cloud observed near the Earth. The aim of the present work is to consider in more detail this disturbance. For this purpose, we used the data available through the Internet (Section 2). The work generally describes the disturbance structure as a whole (Section 3) and studies individual parts of the disturbance: bow shock layer (Section 4), boundary layer (Section 5), magnetic cloud (Section 6), and return shock layer (Section 7). The planetary geoeffectiveness of individual structural elements has been considered in Section 8. Attention is paid to the relation between regional solar sources of this disturbance and large-scale open solar magnetic fields (Section 9) and a comparison is performed with certain characteristics of the solar wind near-Earth disturbances of October 24 and November 22–23, 2003, after the flares from the same active region (Section 10). It is discussed whether it is possible to construct a qualitative scenario of solar–terrestrial storms of a corresponding class (Section 11).

2. SOURCE DATA

We used the IMF and plasma measurements (cdaweb.gsfs.nasa.gov/), the Wilcox Solar Observatory (WSO) measurements of the photospheric magnetic field (quake.Stanford.edu/~wso), and the data on the sporadic phenomena in the active regions and in their vicinities (www.ngdc.noaa.gov/). Moreover, we took into account different data presented in the review by Yermolaev et al. [2005].

3. DISTURBANCE STRUCTURE

On November 20, the near-Earth disturbance structure in the interplanetary medium is reflected in the variations in IMF (B, B_x, B_y, B_z—Fig. 1) and the solar wind plasma (n, n_α/n_p, V, V_x, V_y, V_z, T_p—Fig. 2) according to the ACE satellite measurements (near the forward libration point). Four main structural regions of

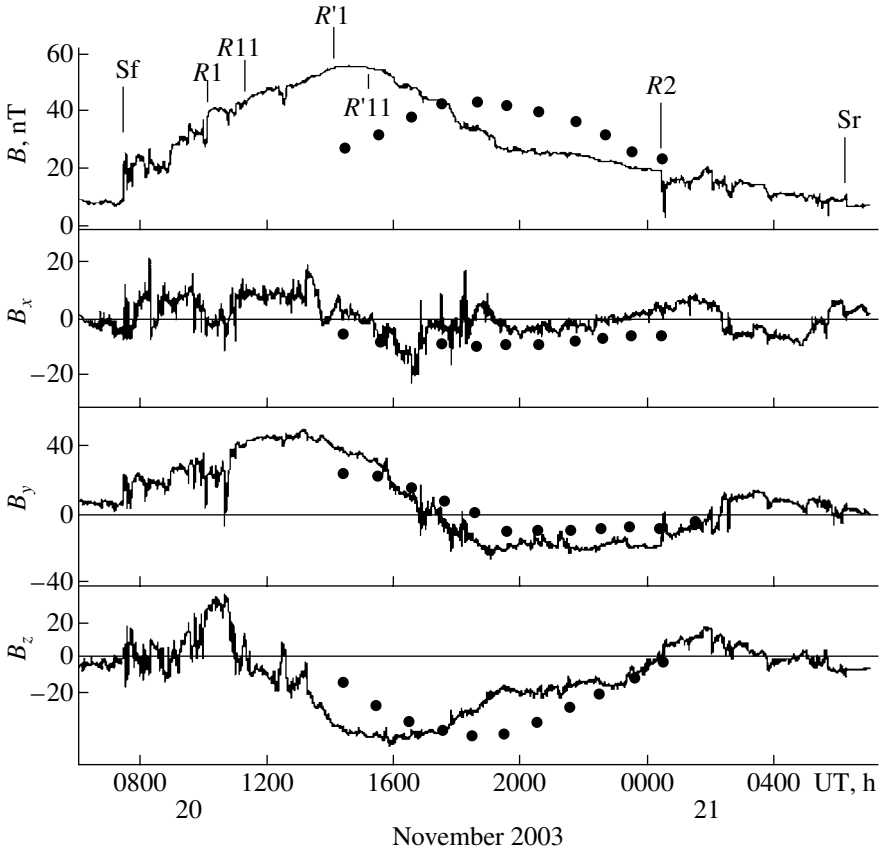

Fig. 1. Variations in the magnetic induction B, B_x, B_y, and B_z (16-s average data, solar–ecliptic coordinates) according to the ACE satellite measurements near the forward libration point (key experimenter N.F. Ness). S_f, R_1, R_{11}, R'_1, R'_{11}, R_2, and S_r are the leading shock front, outer boundary of the boundary layer, boundary between the boundary layer parts with $B_z > 0$ and $B_z < 0$, forward boundary of the magnetic cloud (cavity), forward boundary of the helium domain (filament substance), backward boundary of the magnetic cloud, and return shock front, respectively.

the MHD flow are distinguished: (1) bow shock, (2) boundary layer, (3) magnetic cloud, and (4) return shock.

Table 1 presents the normals to the main strong boundary discontinuities of this disturbance: forward (S_f) and return (S_r) shock fronts and the outer boundary (R_1) of the boundary layer. Figure 3 demonstrates the velocity field in the region of magnetic cloud streamline constructed in the coordinate system stationary relative to the forward shock front.

Table 1. Normals to the strong discontinuities in the MHD disturbances of the interplanetary medium observed on November 20–21 and 22–23, 2003 (φ_N and θ_N are angles in solar–ecliptic coordinates)

Date	UT	Discontinuity	φ_N, deg.	θ_N, deg.
November 20	0726	S_f	176	–7
November 21	1006	R_1	200	8
November 21	0027	R_2	188	16
November 21	0614	S_r	223	0
November 22	1001	S_f	140	–5
November 22	1500	R_1	150	–6

Below, the properties of the above structural regions of the disturbance are considered in more detail.

4. BOW SHOCK (0727–1006 UT)

The bow shock is limited by the shock front (S_f) and discontinuity (R_1) at the boundary layer downstream and upstream, respectively. The substructure (0730–0830 UT) sharply different from the remaining part of the shock layer (0830–1000 UT) in its characteristics is distinguished immediately behind the shock front.

Let us successively consider the properties of these substructures having preliminarily characterized the disturbance front.

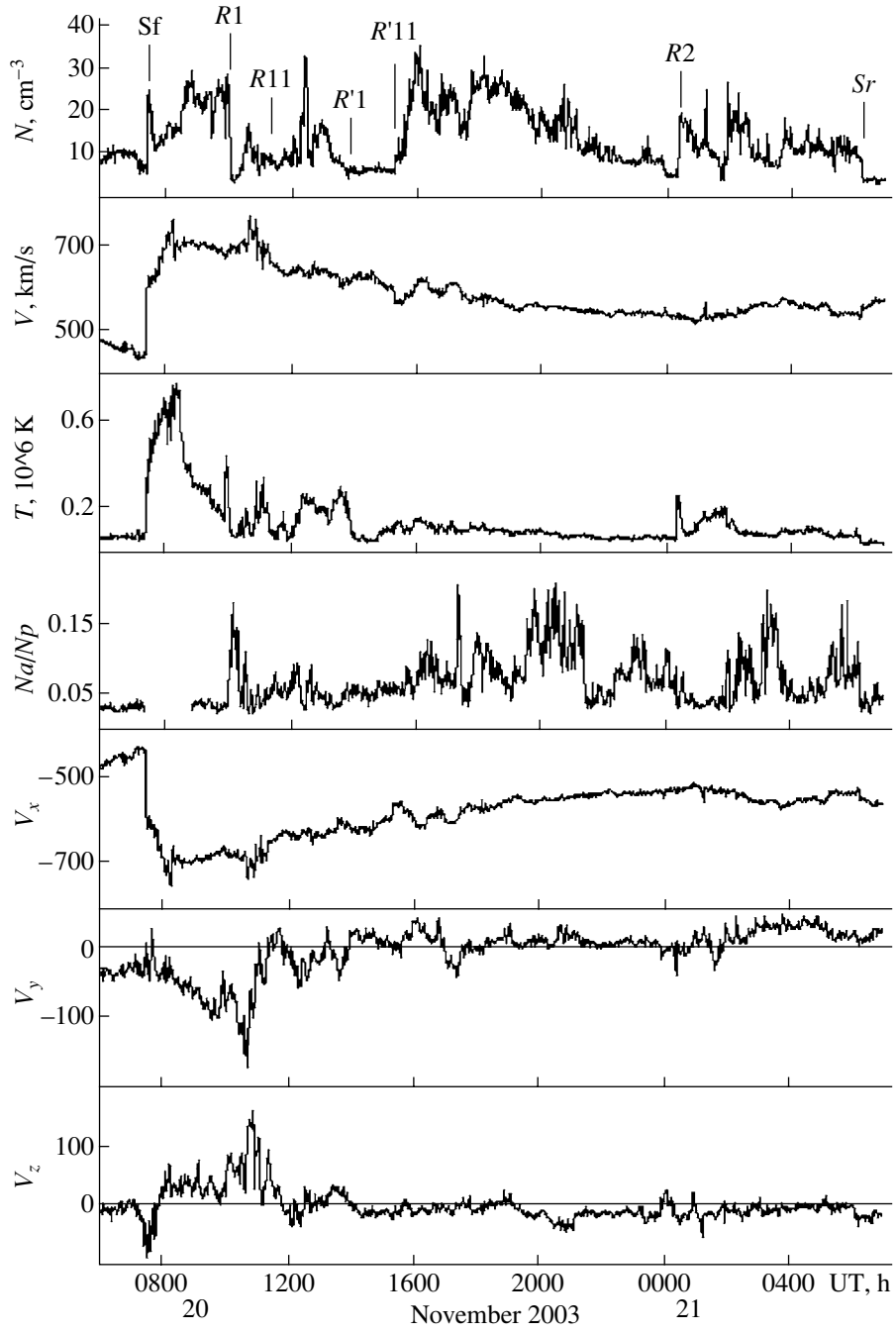

Fig. 2. Variations in the density (N_p), temperature (T), and velocity (V, V_x, V_y, and V_z) of protons and in the abundance ratio of helium nuclei (N_a/N_p) (64-s average data, solar–ecliptic coordinates) according to the ACE satellite measurements (key experimenter D.J. Comas). The denotations are the same as in Fig. 1.

4.1. Forward Shock Front S_f

Based on the ACE satellite measurements performed at about 0727 UT at the point with solar ecliptic coordinates R_1 = (1.5322; 0.169; –0.0592) million kilometers, we can state that the shock front (1) propagated at a velocity of D = 780 km/s (2) in the direction **N** ($\varphi_N = 174°$, $\theta_N = -7°$ (3) at an angle of 50° to the $\mathbf{B}_1$ vector before the front (quasiparallel shock) (4) with a dynamic force that makes it possible to anticipate a cloud field value of $B_m \approx 50$ nT. We also note that the front propagated in the IMF positive sector ($B_x < 0$, $B_y > 0$).

The normal to the front was calculated using the complanarity theorem at $\mathbf{B}_1$ = (–5.5; 6; 1) and $\mathbf{B}_2$ = (–6.8; 19.7; 4.8) nT before and behind the front, respectively. The theoretical propagation time $\tau = (\mathbf{R}_2 - \mathbf{R}_1)\mathbf{N}/D$ from the ACE to Geotail satellites at the point

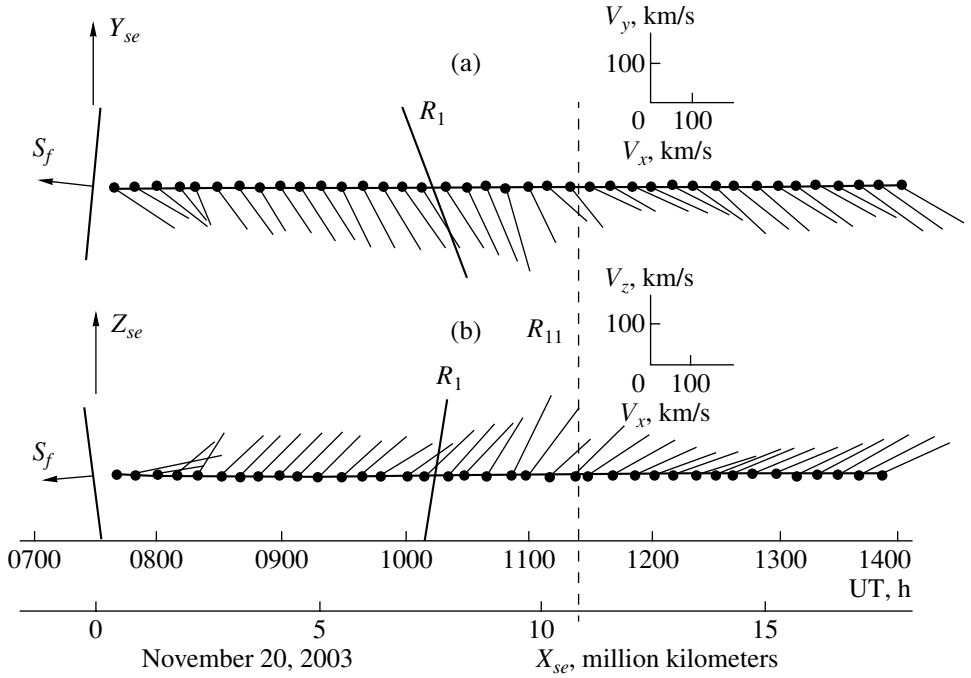

Fig. 3. Variations in the velocity field in the coordinate system immobile relative to the leading shock front S_f (see the text) in the bow shock layer ($S_f - R_1$) and in the boundary layer (behind R_1); (a) and (b) are projections on the planes (X_{SE}, Y_{SE}) and (X_{SE}, Z_{SE}), respectively; straight line is the ACE trajectory; S_f and R_1 are the leading shock front and the outer boundary of the boundary layer, respectively; dashed line (R_{11}) marks the instant of crossing $B_z \approx 0$ in the boundary layer.

$\mathbf{R}_2$ = (0.0173; 0.073; 0.0132) million kilometers equal to 32 min was close to the time (τ^* = 36 min) observed at ~0803 UT on the Geotail satellite.

Thus, the propagation time independently confirms that the **N** (and, consequently, all other characteristics, specifically, the angle between **N** and $\mathbf{B}_1$, calculated based on **N**) was determined correctly.

The front velocity was calculated using the standard formula $D = (n_2\mathbf{V}_2 - n_1\mathbf{V}_1)\mathbf{N}/(n_2 - n_1)$ at a proton density of n_1 = 5.5, n_2 = 19.7 cm^{-3} and $\mathbf{V}_1$ = (–440; –40; –25); $\mathbf{V}_2$ = (–685; –27; –60) km/s.

The anticipated magnetic field value in the cloud was estimated using the formula $B_m = (8\pi m_p n_1)^{1/2}(D - \mathbf{V}_1\mathbf{N})$ based on the assumption that the dynamic impact and magnetic pressure are equal at the cloud boundary proposed many years ago when magnetic clouds (magnetic regions) were uncovered [Ivanov et al., 1974].

4.2 Shock Layer Substructure (0730–0830 UT)

This substructure is located between the shock front and the cold plasma sheet with a sharp front (Figs. 1, 2, 4, 5). The substructure is characterized by a rapid and almost monotonous growth of the velocity and temperature, short-term hook-like rise–fall of the proton density (n) and magnitude (**B**) immediately behind the shock front (0730–0740 UT), and transition from the normal positive IMF sector ($B_x < 0$, $B_y > 0$) into the anomalous sector ($B_x > 0$, $B_y > 0$) at 0750 UT.

Such a combination of variations in V, T, n, B, B_x, and B_y is typical of the layer behind the quasiparallel shock that is formed before an obstacle to be flown around, e.g., before the geomagnetosphere (Figs. 10, 11 in [Spreiter and Alksne, 1968]). In this case one of the components changes its sign due to IMF draping near an obstacle.

4.3. Shock layer substructure (0830–1006 UT)

A dense, hot, and very high-speed and almost stationary (V = const = 700 km/s) plasma flow (Figs. 2, 5) was observed in the shock layer behind its structure considered in Subsection 4.2. Upstream, this flow was limited by a strong discontinuity R_1. The velocity in this substructure, represented in the stationary coordinate system relative to the forward shock front, turned out to be directed along the outer boundary of the boundary layer R_1 (Fig. 3).

In the magnetic field (Fig. 4), B increased mainly due to the B_z value that reached positive values close to maximum ($B_z \approx 30$ nT) at R_1. Beginning from 0930 UT, this growth was modulated by strong fluctuations of all components. Beginning from the same instant, IMF tended to return in the normal positive sector ($B_x < 0$, $B_y > 0$).

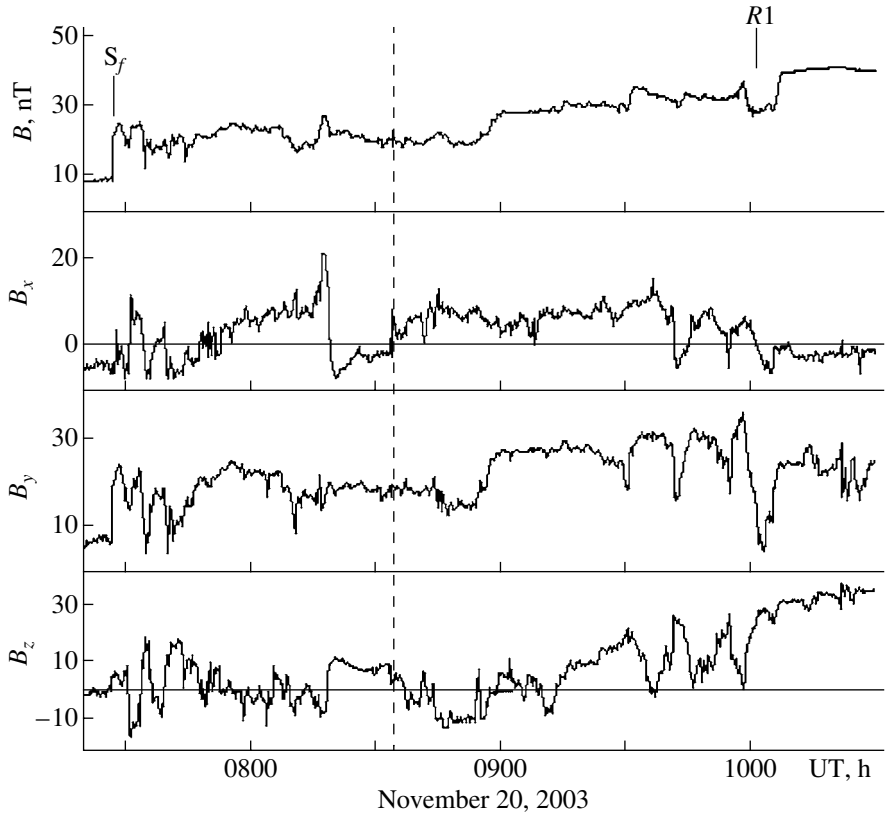

Fig. 4. Variations in IMF in the bow shock layer. The denotations are the same as in Fig. 1. Dashed line shows the boundary between the substructure domains.

Note that the normals to S_f and R_1 proved to be at a considerable angle $\alpha = \arccos(\mathbf{N}_s \cdot \mathbf{N}_R) \approx 28°$.

5. BOUNDARY LAYER (1006–1400 UT)

The boundary layer was observed between R_1 and R_1' (Figs. 1, 2, 6, 7) and had the following substructure: the regions with $B_z > 0$ (1006–1120 UT) and $B_z < 0$ (1130–1400 UT).

5.1. Boundary Layer Substructure with $B_z > 0$ (1006–1120 UT)

This substructure was limited by R_1 and R_{11} downstream and upstream, respectively (Figs. 1–3, 6, 7). At R_1, n_1 sharply decreased and B increased. The normal to R_1 with angles of $\varphi_N = 200°$ and $\theta_N = 8°$ (Table 1) was determined from the ACE satellite data using the scattering matrix method. The substructure was characterized (1) by a very rarefied high-speed hot plasma with unusually considerable (up to ~150 km/s) both smooth and sharp variations in the V_y and V_z velocity components; in this case the velocity in the coordinate system of the forward shock layer was almost parallel to R_1 (Fig. 3); and (2) by the northward IMF B_z component at B = const and by the appearance of sharp changes in B_y and B_z associated with jumps of V_y and V_z,

The set of these characteristics makes it possible to assume that this substructure was the outer part of the boundary layer between the forward shock layer and magnetic cloud.

5.2. Boundary Layer Substructure with $B_z < 0$ (1120–1400 UT)

The substructure with $B_z < 0$ was located upstream of the boundary layer substructure with $B_z > 0$ (between R_{11} and R_1' in Figs. 1–3, 6, 7). At R_{11}, the B_z sign became negative and V relatively smoothly decreased.

The substructure was generally characterized by a gradual increase in $|B_z|$ and B to nearly extreme values (–40 and 52 nT, respectively), a gradual decrease in V and V_y and V_z variation amplitudes, and a sharp change in the velocity direction in the coordinate system stationary relative to S_f (by a deviation of the outer boundary of the boundary layer from the quasiparallel direction (Fig. 3). The latter phenomenon can be interpreted as a plasma reflection from the leading disturbance and, specifically, from R_{11}.

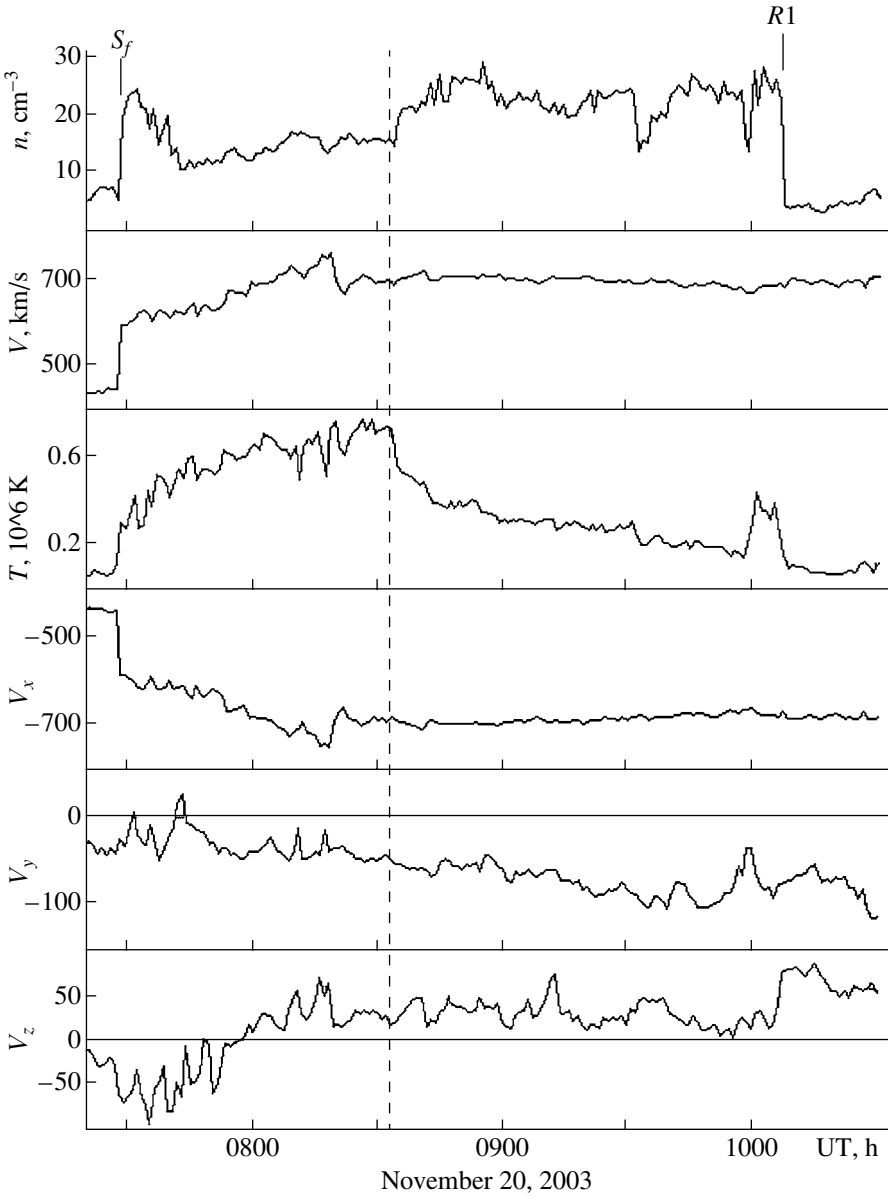

Fig. 5. Variations in the plasma flow in the bow shock layer. Dashed line shows the boundary between the substructure domains. The denotations are the same as in Fig. 2.

6. MAGNETIC CLOUD (1400–0030 UT)

Downstream and upstream of the flow, the cloud is limited by R_1 and R_2, respectively (Fig. 1, 2, 8, 9). Note that the cloud lower boundary could be related to R_{11} since the shock layer substructure with $B_z < 0$ is apparently the outermost cloud part. Magnetic (1400–1520, 2130–0030 UT) and helium (1520–2130 UT) cloud parts can be distinguished between these conditional boundaries according to the initial names of these substructures [Ivanov et al., 1974]. In recent models of solar filament eruption, these substructures could correspond to a magnetic cavity and filament proper [Krall et al., 2000].

6.1. Magnetic domain (cavity) (1400–1520 UT) consists of the leading and tail parts and, thereby, represents the cloud magnetosphere with plasma enriched in helium atoms (plasmasphere). This cavity is characterized by a strong field of a constant value ($B = 56$ nT) and by a rarefied cold and high-speed plasma flow (Figs. 1, 2, 8, 9).

At the R_1' front, mostly westward plasma velocity sharply changes into the eastward velocity ($V_y > 0$) and subsequently remains mainly unchanged. This is possibly the manifestation of the known effect of magnetic cloud pressing out east of the radial propagation due to the ambient counterpressure [Cosling et al., 1987].

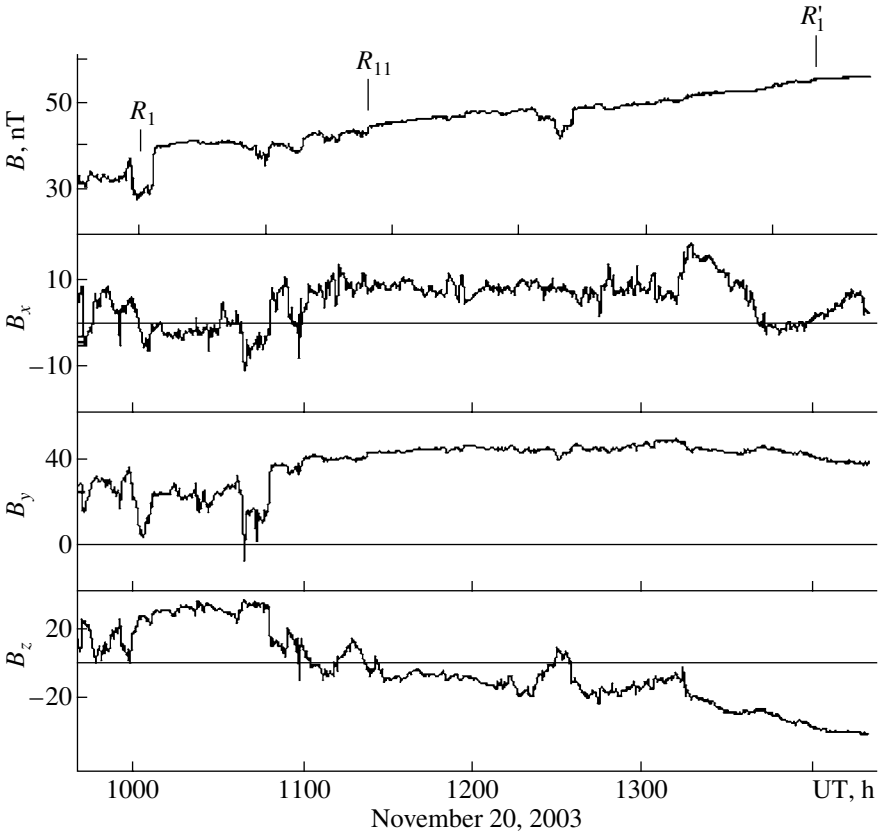

Fig. 6. Variations in IMF in the boundary layer. The denotations are the same as in Fig. 1.

6.2. Helium domain (filament) (1520–0030 UT) is characterized by a dense plasma enriched in helium atoms (Figs. 2, 9). At the R_{11}' boundary, magnetic induction starts gradually decreasing in parallel with an increase in the density (n). Moreover, velocity decreases and temperature increases in discrete steps, although insignificantly. Since the temperature rises, to coordinate with the assumption that the helium domain includes a filament substance, it should be assumed that this substance warms up when propagating in the interplanetary medium [Yermolaev et al., 2005].

Within the helium domain, the ratio n_α/n_p is rather unstable and reaches its maximal values in the interval 1930–2130 UT, i.e., in the middle of this domain, and the density (n_p decreases in the interval 2100–2230 UT, i.e., long before the R_2 boundary is reached. Taking these properties into account, we can assume that the helium plasma is packed within the magnetic domain. A strong discontinuity (R_2) separates the magnetic cloud from the return shock layer. The normal to R_2 was determined from the condition $\mathbf{N} \uparrow\uparrow \mathbf{B}_1 \times \mathbf{B}_2$ and proved to be parallel to the normal to the outer boundary R_1 of the boundary layer (Table 1).

6.3. Magnetic Cloud Model

The variations in B, B_x, B_y, and B_z are theoretically presented (dots in Fig. 8) in the model of the force-free field of a circular cylinder with the axis directed southward ($\varphi_a = 0°$, $\theta_a = -90°$), right-handed helicity, and radius and sighting distance of $R_0 = 10.6$ and $Y_0 = 1.84$ million kilometers, respectively. In this model $B_x = B_0 Y_0 J_1/R$; $B_y = B_0[1 - (Y_0/R)^2]^{1/2} J_1$; $B_z = B_0 J_0$, where $B_0 = 45$ nT, and J_0 and J_1 are the Bessel functions of the first kind of zero and first orders of argument $2.4R/R_0$ (R is the variable distance from the satellite to the cloud center). At such a configuration, the cloud is oriented along the meridian and is almost parallel to the plane of the heliospheric current sheet (Fig. 10).

It is clear that this model approximately represents actual field profiles in this cloud.

7. RETURN SHOCK (0030–0614 UT)

The structural region between R_2 and S_r (Figs. 1, 2) could be supposedly characterized as a shock according to the following criteria: upstream of S_r, the n, T, and B values decrease and velocity (V) increases, which qualitatively corresponds to anticipated changes for a fast magnetosonic front propagating sunward over the solar wind plasma particles.

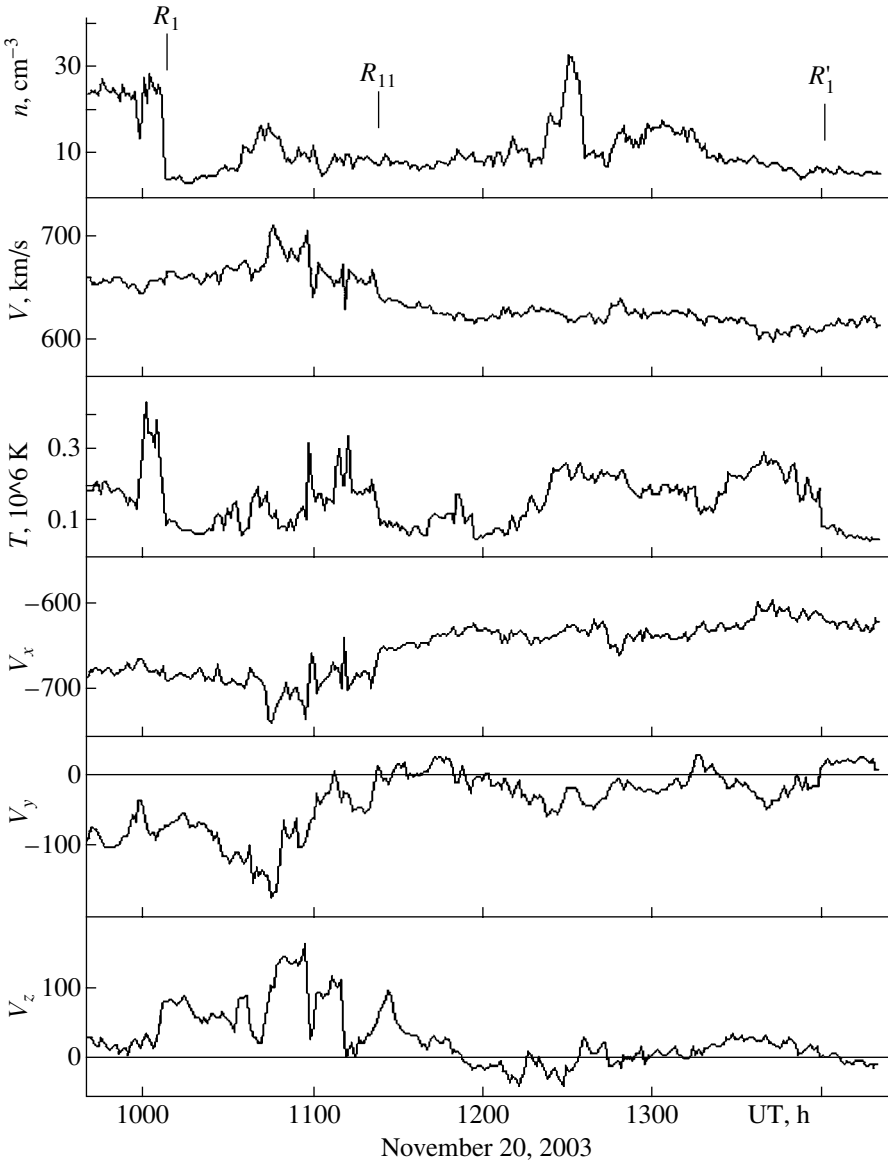

Fig. 7. Variations in the plasma flow in the boundary layer. The denotations are the same as in Fig. 2.

The normal to S_r determined using the scattering matrix method was directed at angles of $\varphi_N = 43°$, $\theta_N = 0°$. Such a direction of the normal disagrees with the assumption that S_r is a shock front since $V_{N1} = V_{N2}$ in this case. Successive substructures in the negative ($B_x > 0$, $B_y < 0$) and positive IMF sectors, correspondingly, in the intervals 0030–0220 and 0220–0540 UT can be distinguished in the layer. The IMF negative sector is finally formed soon after crossing S_r (~0700 UT).

8. DISTURBANCE MHD STRUCTURE AND GEOMAGNETIC ACTIVITY

Judging by the *Dst* index of geomagnetic activity (–472 nT), this storm intensity was the second for the entire history of observations [Yermolaev et al., 2005]. According to the daily A_p index, planetary geomagnetic activity was equal to 150 [ftp:ftp.gfz-potsdam.de/pub/home/obs/kp-ap].

Table 2 shows in more detail the relationship between the MHD structure of the solar wind disturbance and the 3-h planetary index (a_p).

It is clear that the a_p dynamics was governed by the disturbance MHD structure. When the Earth was located in the bow shock layer, the a_p value corresponded to a very large geomagnetic storm. This activity level remained in the first half of the boundary layer (with $B_z > 0$) and became twice higher, reaching the extra storm level, in the second half of this layer (with $B_z < 0$). Activity almost doubled again when the geomagnetosphere crossed the magnetic cloud. Activity

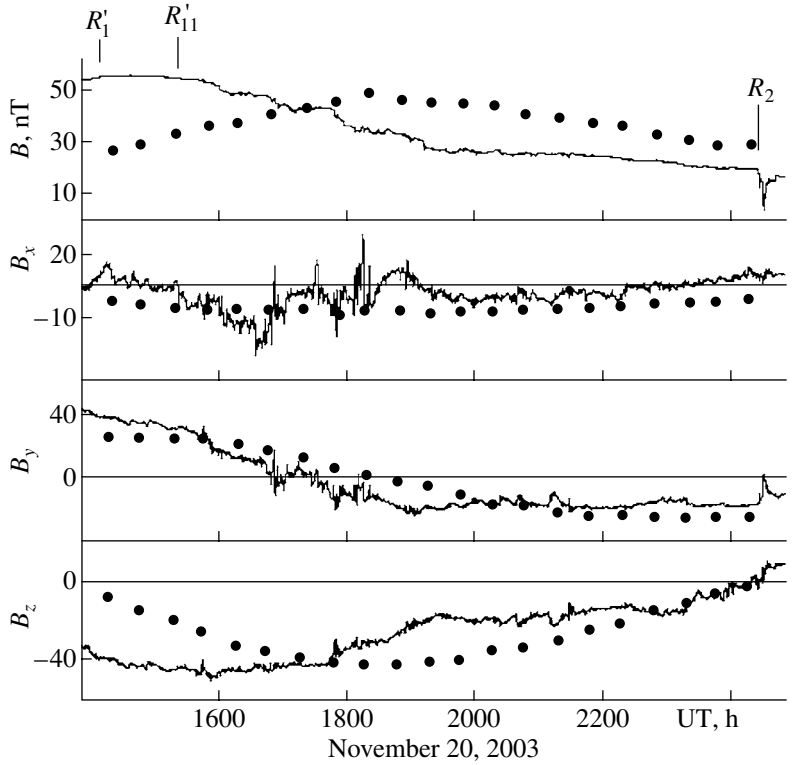

Fig. 8. Variations in IMF in the magnetic cloud. Dots are the model values of the force-free field (see the text). The denotations are the same as in Fig. 1.

started gradually decreasing in the magnetic cloud tail (2100–2400 UT) when the helium domain was left (Subsection 6.2). In the return shock layer, a_p continued decreasing to the level of a very large storm (0300–0600 UT), and the storm intensity decreased from very high to low 3 h after the exit from this layer (0900–1200 UT, November 21, 2003).

9. SOLAR SOURCES

According to our approach to studying solar sources of solar–terrestrial storms [Ivanov et al., 2005], it is desirable to consider the dynamics of the large-scale open solar magnetic field (OMF) and of the field of velocities before the storm commencement, to determine the complex of activity destabilization of which caused the coronal–interplanetary disturbance, to determine the relation between this complex and large-scale fields, and to adjust the complex to the near-Earth disturbance.

A complete realization of this program is outside the scope of this work, and we will consider below only certain concepts to be used in the discussion (Section 11).

9.1. Large-scale Fields and Complex of Activity

Solar sources of this storm were located in the main zone of active longitudes in the OMF negative sector near the westward branch of the OMF zero line (Fig. 10). The sector expanded in longitude, and OMF photospheric sources exerted corresponding divergent motions (Tables 2, 3; Fig. 1 in [Ivanov et al., 2005]). The flare-active region AR 10501 associated with

Table 2. Geoeffectiveness (a_p index and planetary storm class) of the structural domains of the interplanetary MHD disturbance (bow shock layer, BSL; boundary layer, BL; magnetic cloud, MC; return shock layer, RSL)

Date	UT	Structure	a_p	Class
November 20	0000–0300	–	4	Quiet
	0300–0600	–	22	Low
	0600–0900	BSL	94	Very high
	0900–1200	BL	94	Very high
	1200–1500	BL	179	Extra
	1500–1800	MC	300	Extra
	1800–2100	MC	300	Extra
	2100–2400	MC	207	Extra
November 21	0000–0300	RSL	111	Extra
	0300–0600	RSL	80	Very high
	0600–0900	–	80	Very high
	0900–1200	–	22	Low

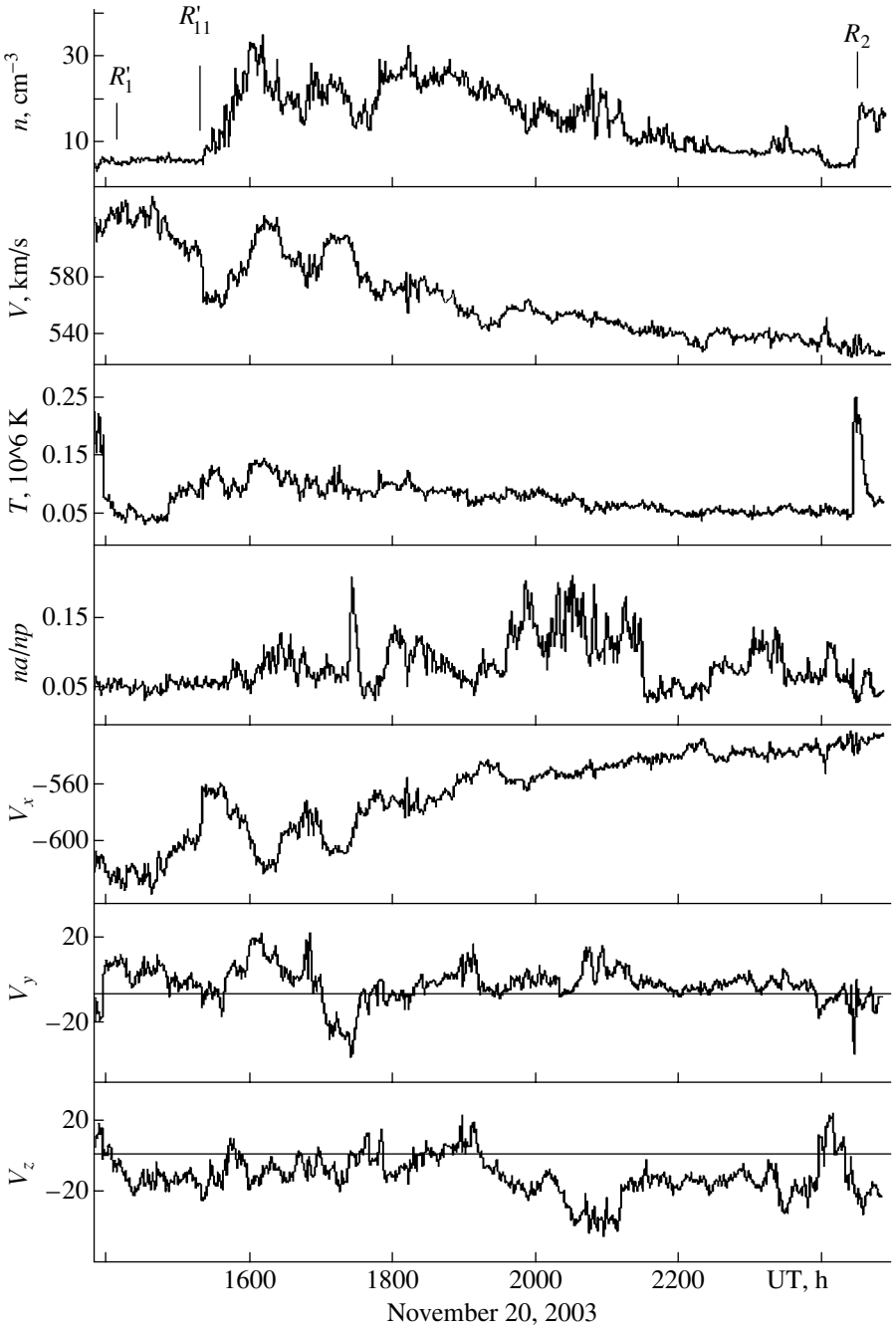

Fig. 9. Variations in the plasma parameters in the magnetic cloud. The denotations are the same as in Fig. 2.

active filament was located between the permanent coronal hole and the OMF zero line (Fig. 10). The series of flares and filament eruption were observed in this region near the Earth helioprojection (Table 3). Thus, this storm originated in a complicated activity complex and can be classified as a flare–hole–filament–streamer storm [Ivanov, 1996, 1998].

It is also interesting that the center of AR 10464 ⟶ 10484 systematically shifted along the heliolatitude during two previous rotations (**Φ** = 05N ⟶ 02N) (Table 2 in [Ivanov et al., 2005]), and active filament originated in the leading part along the AR motion.

9.2. Relation between the Solar Sources and the Near-Earth MHD Disturbance of the Solar Wind

This relation will become completely clear if we manage to determine how similar characteristics of the solar activity complex responsible for this disturbance

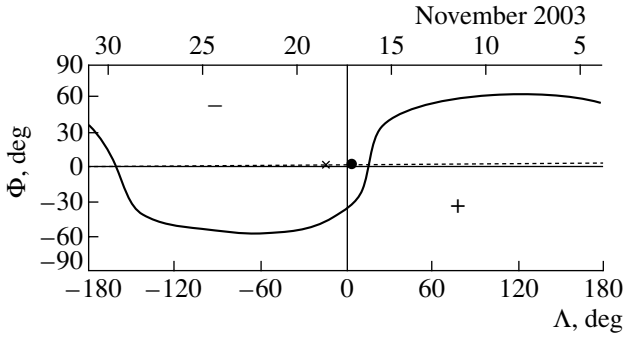

Fig. 10. Zero curve of the open solar magnetic field on the source surface and positions of the flare (cross) and the Earth (dot). Plus and minus are the signs of the sector structure.

are reflected in the structure, configuration, and dynamics of the near-Earth MHD disturbance. This specific event remains evidently unclear in many respects. We note two concepts that will be useful in the discussion of the possible scenario of this storm. First, the storm on the Sun originated near the OMF zero line (Fig. 10), and the near-Earth MHD disturbance was observed at the corresponding IMF sector boundary (Section 4). Second, we would like to pay attention to an approximate parallelism between the transient hole originated after the filament eruption near AR 10501 (Fig. 6 in [Yermolaev et al., 2005]), the OMF zero line (Fig. 10), and the magnetic cloud axis when this cloud passed near the Earth orbit (Section 6).

10. THREE STORMS FROM ONE ACTIVITY COMPLEX WITH AR 10484 (10501)

The storms of October 24, November 20, and November 22, 2003, originated in the same activity complex with AR 10484 (10501) are compared below. The idea of these comparisons is as follows.

(1) The storms of October 24 and November 20, 2003, were recurrent with an almost identical relative position of the active region, OMF zero line (heliospheric current sheet, HCS), and Earth helioprojection. Therefore, a comparative study of the previously obtained data on the storm of October 24, 2003 [Ivanov et al., 2005] and the data on the storm of November 20, 2003, obtained above make it principally possible to determine the general and specific characteristics of these particular storms and to make certain conclusions on the properties of such storms as a whole.

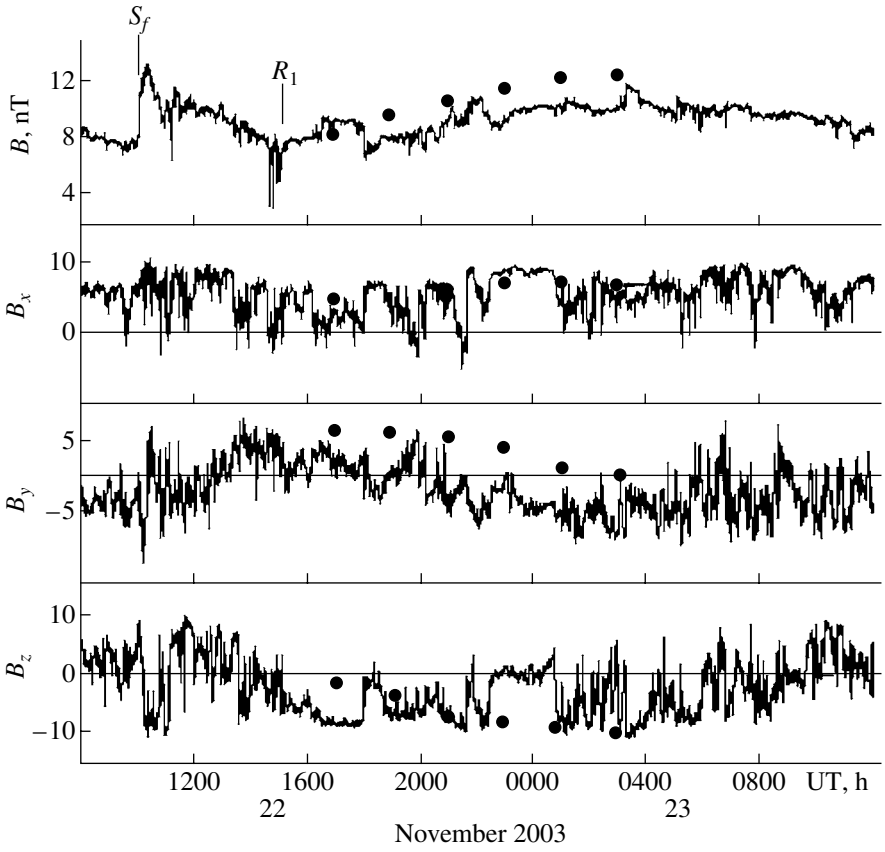

Fig. 11. IMF variations according to the ACE satellite measurements after the 2b(M9.6) flare on November 20, 2003; S_f and R_1 are the leading shock front and the magnetic cloud boundary, respectively. Dots show the field model values.

Table 3. Flares and filaments in AR 10484 (10501)

AR	Date	UT	Class	Φ, deg.	Λ, deg.
10484	October 20	0648	2*n*	04N	46E
	October 22	1507	*sn*	05N	22E
	October 22	1559	*sn*	03N	17E
	October 23	0236	*sn*	03N	15E
10501	November 17	0859	1*n*	01S	33E
	November 18	0716	2*n*	00N	18E
	November 18	0723	*DSF*	00N	18E
	November 19	0759	1*f*	03N	01E
	November 20	0355	1*n*	01N	06E
	November 20	07:38	2*b*	01N	08W

(2) The storms of November 20 and 22, 2003, represent the series of storms that were observed during and after HCS crossing and followed the flares of almost identical power from the same AR 10501. Therefore, a comparison of these storms can give results similar to those anticipated during multisatellite observations of the same disturbance.

A detailed comparison falls outside the scope of this paper; therefore, we briefly pay attention to the following circumstances.

10.1. Storms of November 20 and October 24, 2003

The identical relative position of AR, HCS, and the Earth apparently resulted in that the identically directed normals to the leading shock fronts (Table 1) and to the outer magnetic field and very similar variations in V_x, V_y, and V_z (Figs. 1, 5 in this paper; Fig. 3 from [Ivanov et al., 2005]) make it possible to conclude that the velocity fields in the bow shock layers of these two disturbances were to a certain degree similar (reproducible).

The set of more powerful sporadic phenomena in AR 10501 (the storm of November 20) as compared to such phenomena in AR 10484 (the storm of October 24) (Table 3) could cause a higher shock velocity D (November 20), a higher dynamic impact on an obstacle, and, as a consequence, a larger magnitude $B_m = (8\pi m_p n_1)^{1/2}(D - \mathbf{V}_1\mathbf{N})$ in the clearly defined magnetic cloud of November 20 (Fig. 1) instead of a small fragment of this cloud during the storm of October 24, 2003 (Fig. 2 in [Ivanov et al., 2005]).

Judging by the data of the SOHO MDI instrument, a strong difference in the configuration of the magnetic fields in ARs 10484 and 10501 could principally cause a different configuration of the field in the corresponding near-Earth clouds.

10.2. Storms of November 20 and 22, 2003

During these two events, MHD disturbances were observed before and behind HCS, respectively. These disturbances followed the 2*n* flare and filament eruption and the 2b western flare, respectively (Table 3). The intensity of the MHD disturbance of November 22 was low in almost all parameters (Figs. 11, 12). The shock front propagated at a low velocity almost along $\mathbf{B}_1$, and a low dynamic impact did not lead to a considerable increase in B_m in the magnetic cloud, as a result of which it was apparently difficult to identify this cloud. Figure 11 shows the cloud boundaries and its model field at the same orientation of the cloud axis ($\varphi_a = 0°$, $\theta_a = -90°$) as for the cloud in the MHD disturbance of November 20, 2003 (Fig. 8).

11. DISCUSSION

This paper continues studying the solar–terrestrial storm of November 18–20, 2003 [Yermolaev et al., 2005] in two following directions: (1) to study in more detail the structure, configuration, and dynamics of the near-Earth disturbance and to relate this disturbance to solar sources; (2) to develop the scenario of the solar–terrestrial chain of the physical processes responsible for this storm.

Below we present results of the first direction of the study and assess their novelty, reliability, and significance. Based on these results, we propose the possible scenario of this storm and especially stress on the explanation of its high power.

11.1. Summary of the Results and Their Assessment

The solar–terrestrial storm of November 18–20, 2003, belong to the wide class of storms that originate near the zero line of the coronal open solar magnetic field and are observed on the heliospheric current sheet (HCS) in the near-Earth space. In Section 9 this storm is classified as a complicated flare–hole–filamentary–streamer event based on the consideration of the corresponding activity complex structure [Ivanov, 1996, 1998]. The interest to storms on HCS progressively increases, and, as a consequence, the literature devoted to these storms is very extensive (see references in [Ivanov et al., 2005]). However, detailed studies of these storms, using the entire set of data and including the construction of the phenomenological scenario of the phenomena from the Sun to the Earth, are still at the very beginning: [Tokumaru et al., 2003]—the storm of July 15, 2000; [Yermolaev et al., 2005]—the storm of November 20, 2003. Ivanov et al. [2005a] proposed the qualitative scenario of the physical processes and the schematic model for the storm of July 15, 2000, based on a detailed consideration of the complex of phenomena.

Recall that Yermolaev et al. [2005] referred to the shock and magnetic cloud in the structure of the disturbance observed on November 20, generally related the disturbance to sporadic phenomena in AR 10501, and were interested in the origin of the unusual combination

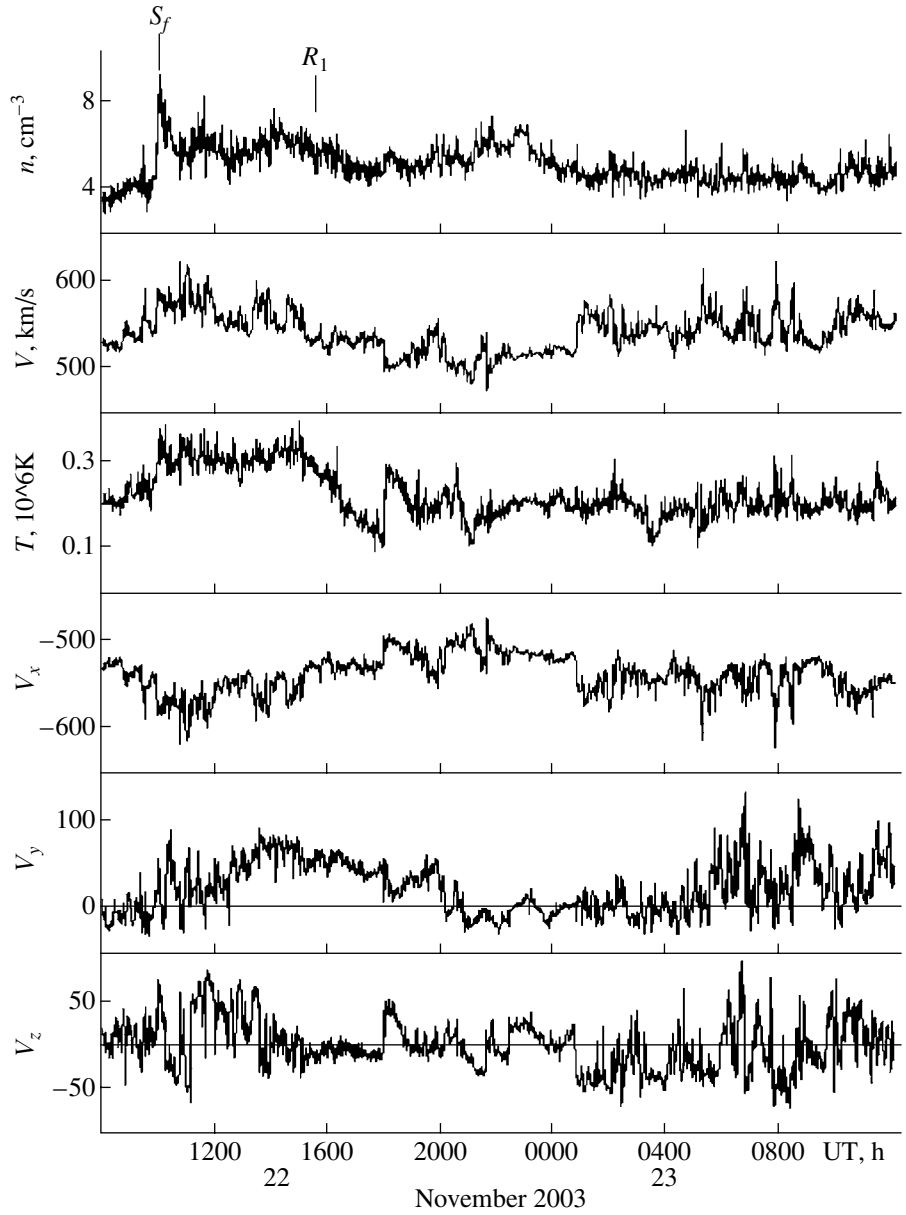

Fig. 12. Variations in the solar wind plasma parameters according to the ACE measurements. The denotations are the same as in the previous figures.

of a large field and dense hot plasma within the magnetic cloud.

Above we determined the leading shock front characteristics, identified the shock layer substructure, detected a wide boundary layer in going from the shock to the cloud, and determined the cloud axis direction. In these studies we applied the method for constructing the field of disturbed velocities in the coordinate system stationary relative to the shock front along with the standard technique used to separate the disturbance into structural domains, to determine the boundaries of these domains, and to elucidate their hydrodynamic sense. Moreover, we compared this storm with two other storms from the same complex of activity: (1) with the storm of October 24, 2003, at an identical relative position of AR, HCS, and the Earth, when both MHD disturbances in the near-Earth space were observed before and during HCS crossing; (2) with the storm of November 22, 2003, when the Earth was located on two different sides of HCS and AR 10501 (before HCS crossing and west of AR on November 20 and October 24, 2003; after HCS crossing and east of AR on November 22, 2003). Such an approach made it possible to reveal the reproducibility of the field of velocities and the geometry of shocks in the first case and to sound two disturbances of a close origin from two sides: before and after HCS crossing.

1. The shock front on November 20, 2003, rapidly moved quasiparallel to the $\mathbf{B}_1$ field almost in the plane of ecliptic and parallel to the Sun–Earth line. It was found out that these characteristics (except the velocity value) almost exactly reproduce the characteristics of the front on October 24, 2003 [Ivanov et al., 2005] at an identical position of the satellite relative to AR and HCS. A high front velocity (D) on November 20, 2003, is naturally explained by a higher power of the corresponding sporadic phenomena. These shock front characteristics were used, first, to estimate the field value in the magnetic cloud $B_m = (8\pi m_p n_1)^{1/2}(D - \mathbf{V}_1\mathbf{N})$. This formula was proposed many years ago when magnetic clouds (domains) were discovered [Ivanov et al., 1974]. Having been obtained from the conditions of equality of a hydrodynamic impact on a cloud and a magnetic pressure at a cloud boundary, this formula clearly indicates the origin of large B_m in a cloud and can be used in a short-term prediction of B_m. Second, the data on $\mathbf{N}$ and D made it possible to study the velocity field behind the shock front in the coordinate system immobile relative to this front, which was performed for the first time as applied to interplanetary disturbances. In this case it was for the first time indicated that the velocity field in the shock layer is parallel to the boundary of a flown-around obstacle and increases within the boundary layer. Third, a quasiparallel character of the shock makes it possible to qualitatively explain the variations in B, B_x, and n in the shock layer substructure adjacent to the front.

In the results of studying the shock layer, we pay attention to two unclear circumstances. First, if a change of the B_x sign behind the shock front is explained by IMF draping near a flown-around obstacle, as is done in the model of a stationary flow around the magnetosphere behind the quasiparallel shock [Spreiter and Alksne, 1968], it is unclear why draping is not confined only to a narrow layer before an obstacle. Actually, $B_x > 0$ and $B_y > 0$ in almost the entire shock layer except a narrow zone immediately behind the shock front. Second, it is unclear why the angle between the normals to the shock front S_f and to the outer boundary of the boundary layer R_1 reaches ~30°.

Both these unclear circumstances can supposedly be explained by the fact that the flow is nonstationary, although the errors in determining the normals (especially, to R_1) could also be substantial in the latter case. The boundary layer behind the R_1 boundary between the shock and cloud (Section 5) proved to be unusually wide as compared to the known layer [Ivanov, 1984] composed of two parts with oppositely directed B_z components, which makes it possible to assume that reconnection of the cloud and shock layer fields takes place in this case. In the outer part of the boundary layer, $B_z > 0$ and the velocities, parallel to R_1, increase; in the inner part (in the cloud), $B_z < 0$ and the velocities change their direction so that plasma is supposedly reflected from the boundary between these parts where the B_z component crosses zero. The boundary layers on magnetic clouds, especially so unusual, are still almost unstudied.

Magnetic cloud is represented by a circular cylinder with the axis directed along the meridian and parallel to HCS. The magnetic domain (magnetosphere) and the helium domain (plasmasphere), with a dense plasma enriched in helium, packed in the magnetosphere are distinguished in the cloud structure. This structure quite corresponds to the earliest description of a magnetic cloud [Ivanov et al., 1974] and to the recent concepts of solar magnetic ropes containing a filament material [Krall et al., 2000].

The presence of magnetic clouds in the near-Earth disturbances of October 24 and November 22, 2003, is still problematic. However, as was shown in Section 9 and in [Ivanov et al., 2005], the available data do not rule out the following conclusions. (1) The fragment of the magnetic cloud with $B_m = (8\pi m_p n_1)^{1/2}(D - \mathbf{V}_1\mathbf{N})$ but with an absolutely different field orientation ($B_z > 0$) than in the cloud of November 20, 2003, was observed on October 24, 2003, when the position of AR–HCS–satellite was the same as during the storm of November 20, 2003. (2) The magnetic cloud, where B_m was very small but satisfied the above formula and the cloud axis direction was the same as in the cloud of November 20, 2003, was observed on November 21–22, 2003, when the satellite was located east of HCS and AR in contrast to November 20, 2003.

These assumptions should be subsequently substantiated; nevertheless, we will use them below in constructing the qualitative physical scenario of the storm observed on November 18–20, 2003.

11.2. Scenario of the Solar–Terrestrial Storm of November 18–20, 2003

By scenario we mean the spatial–temporal regulation of the entire complex of storm phenomena assuming a logical interpretation, which gives the knowledge of the series of physical processes of generation and destabilization of the activity complex and origination and passage of the disturbance in the coronal–interplanetary medium. We developed such a scenario for the known storm of July 15, 2000, the results of which are presented in four papers. For this purpose, we had to consider the dynamics of large-scale open solar magnetic fields [Ivanov and Kharshiladze, 2004], its relation to the sunspot velocity field [Ivanov, 2004a], the processes in the corresponding AR and their relation to large-scale fields [Ivanov, 2004b], and the complex of coronal and interplanetary phenomena [Ivanov et al., 2005a]. In the last work, we generalized the results of many particular studies of this storm along with primary data.

It is untimely to perform such a work concerning the storm of November 18–20, 2003, in full measure since

profound particular studies are still at the very beginning in spite of the presence of a detailed data review [Yermolaev et al., 2005]. However, we will indicate below that it is already possible to develop a certain preliminary scenario of this storm to be used in the future work. The problem is facilitated by the presence of the scenario for the storm observed on July 15, 2000, the main points of which are given in [Ivanov et al., 2005] and are as follows:

(i) Convergent motion of large-scale antiparallel magnetic fields with the formation of a powerful sunspot group, involved in a rigid corotation together with the active sector boundary against the inertia forces of differential rotation, between these fields below this boundary.

(ii) Formation of an active filament in the leading part of AR and adjustment of the neutral line of the AR photospheric magnetic field to the sector boundary direction at the phase of energy accumulation in AR.

(iii) Successive ejections of filament and magnetic rope with the formation of an ellipsoidal transient coronal disturbance whose axes were directed along and across the sector boundary.

(iv) Rapid one-sided extension of the coronal disturbance along the sector boundary.

(v) Self-similar disturbance propagation in the interplanetary medium with the appearance of the magnetic cloud, whose axis was parallel to the sector boundary, near the Earth.

We can assume that this scenario, developed for the storm of July 15, 2000, is to a certain degree applicable to the storm of November 18–20, 2003. Data that can be used to verify this assumption are still insufficient, especially as applied to the storm early phases. However, the filament origination and eruption, almost simultaneous with the flare, is emphasized [Yermolaev et al., 2005]. We would like to pay attention to the fact that the configuration of the leading part of this filament (Fig. 2 in [Yermolaev et al., 2005]) was similar to the configuration of the southeastern part of the nearest HCS branch (Fig. 10). The transient coronal hole (dimming) formed after eruption was first a small localized formation and then rapidly extended mostly southeastward (Fig. 6 in [Yermolaev et al., 2005]). On the whole, the configurations of the filament, dimming, and the nearest HCS branch corresponded to the configuration of the coronal mass ejection at altitudes $r = 1.6R_s$ (Fig. 4 in [Yermolaev et al., 2005]).

In the model of the near-Earth magnetic cloud, the axis was parallel to the HCS plane and meridian. This axis could be turned southeastward, parallel to the neutral line of the open field on the source surface, within the errors of modeling. Thus, the axes of symmetry of the active filament, transient hole, coronal ejection, and the nearest HCS branch, as well as the magnetic cloud axis, proved to be almost parallel during the storm of November 18–20, 2003. A similar parallelism in the different-scale structural formations from the Sun to the Earth was also observed during the storm of July 15, 2000 [Ivanov et al., 2005a] and apparently results from the interaction between proper small-scale open AR fields and large-scale fields [Ivanov, 2004a, 2004b]. Note that a parallelism of the photospheric field zero line (in active regions) and the longitudinal axis of the coronal mass ejection at distances of 1.5–6R_s (LASCO coronograph, C2) follows from the static studies of CME observations in 1996–2002 and is reflected in the CME phenomenological model (Fig. 15 in [Cremades and Bothmer, 2004]).

One of the differences between the storms of July 15 and November 20 consists in that the active regions were located below the open field zero line (HCS) and outside this line at a distance of almost 30° in longitude, respectively (Fig. 10). Consequently, CME interacted with HCS from the very beginning in the first case and had to collide with HCS during its propagation through the corona and interplanetary medium in the second case. We can assume that this is, specifically, the difference between the considered storm scenarios. At the beginning of the storm of November 18–20, 2003, the collision between CME and HCS could cause a large field in the near-Earth MHD disturbance because of a strong suppression of shocks reflected from HCS [Ivanov, 1981]. Below we present the idealized model of direct shock reflection from a rigid wall [Tsintsinadze and Loladze, 1963; Ivanov, 1981a] illustrating this effect.

Heliospheric streamer (HCS), which is successively flown around by shocks after these flares, plays the role of a rigid wall. Magnetic plasma pressure on HCS increases and energy is pumped into the magnetic field as a result of shock suppression.

We now briefly recall the calculation scheme that makes it possible to estimate the effects of this interaction [Ivanov, 1981, 1981a].

1. A shock S_{f1} flowing around HCS (Fig. 13a) is characterized by the Mach numbers

$$M_1 = (D - V_{n1})(\gamma m_p/kT_{p1})^{1/2},$$

$$M_{A1} = (D - V_{n1})(4\pi m_p n_1)^{1/2}/B_1.$$

The jumps of the values $\sigma_{21} = n_2/n_1 = B_2/B_1 = (D - V_{n1})/(D - V_{n2})$ and the wave amplitude $\tau_{21} = p_2/p_1$ are calculated from the formulas

$$\sigma_{21} = \frac{6M_1^2M_{A1}^2}{2M_1^2M_{A1}^2 + 6M_{A1}^2 + 5M_1^2 + [(2M_1^2M_{A1}^2 + 5M_1^2)^2 + 128M_{A1}^2M_1^4]^{1/2}},$$

$$\tau_{21} = \frac{3\sigma_{21}M_{A1}^2 + (\sigma_{21}-1)[(\sigma_{21}-1)M_{A1}^2 - 2\sigma_{21}^2]M_1^2}{3M_{A1}^2}.$$

2. A stable reflected wave S_r with the amplitude $\tau_{32} < \tau_{21}$ but with $n_3 = \sigma_{21}\sigma_{32}n_1 > n_2$, $B_3 = \sigma_{21}\sigma_{32}B_1 > B_2$, and $p_3 = \tau_{21}\,\tau_{32}p_1 > p_2$, where

$$\sigma_{32} = 1 + 2\left[\frac{8\pi\tau_{21}}{3\sigma_{21}^2}\left(\frac{\gamma+1}{\gamma-1}\tau_{32}\right)\frac{p_1}{B_1^2}\right]^{1/2} \times \sinh\frac{1}{3}\operatorname{arcsh}\frac{24\sqrt{3(\gamma-1)}\pi\tau_{21}(\tau_{32}-1)p_1}{\{8\pi\sigma_{21}\tau_{21}[(\gamma+1)+(\gamma-1)\tau_{32}]p_1B_1\}^{3/2}},$$

$$\tau_{32} = 1 + G + \left[\left(1 - \frac{1}{\tau_{21}} + G\right)^2 + \frac{\sigma_{21}(\sigma_{21}-1)(\tau_{21}-1)B_1^2}{2\pi\tau_{21}\pi_1}\right]^{1/2},$$

$$G = \frac{\gamma+1}{16\pi\tau_{21}}\frac{8\pi(\tau_{21}-1)^2p_1 + (\tau_{21}-1)(\sigma_{21}^2-1)B_1^2}{\gamma(\tau_{21}+1)p_1 + (\tau_{21}-1)p_1 + (\sigma_{21}-1)^2B_1^2} - \frac{(\sigma_{21}-1)(3\sigma_{21}-1)B_1^2}{16\pi\tau_{21}p_1}$$

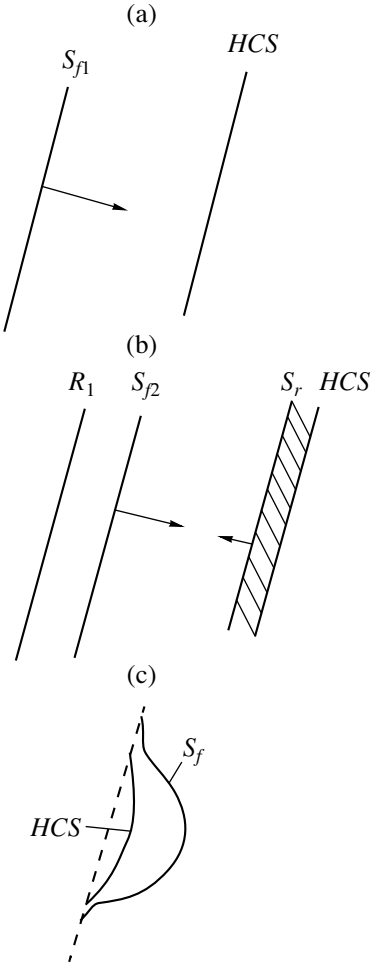

Fig. 13. The scheme illustrating the interaction between shock waves and HCS: (a) S_{f1} wave flow around HCS; (b) S_{f2} wave flow around HCS with the reflected wave S_r; and (c) refracted wave front S_f and HCS bend.

is formed after collision with HCS (rigid wall) (Fig. 13b).

Yermolaev et al. [2005] assumed that large B and T in the magnetic cloud of November 20 could result from the superposition of successive disturbances. One of the possible specific mechanisms, for the first time considered and numerically estimated by Ivanov [1981] as a mechanism of generation of interplanetary extra disturbances, was indicated above.

However, HCS is not an absolutely rigid wall: a refracted shock crosses HCS, and this sheet is elastically distorted (Fig. 13c). This phenomenon is first of all reflected in the presence of a bow (refracted) shock S_f registered (Fig. 13c) before HCS crossing and, possibly, in a considerable angle between the normals to the S_f front and the boundary layer. In the course of earthward propagation, this angle should decrease because HCS is pressed out eastward due to the dynamic impact on the magnetic cloud.

A similar scenario is applicable to the storm of October 20–24, 2003, since the relative position of AR 10484 and HCS was the same as the position of AR 10501 and HCS during the storm of November 17–20, 2003. We can assume again that shocks caused by the series of flares flow around HCS, and pressure (including magnetic one) increases behind reflected waves as a result of shock suppression. Refracted waves form the leading shock front and distort HCS; satellites register almost identical variations in the velocity field in an identical position relative to the AR–HCS complex. Differences in the storm structure and intensity depend on differences in the series of sporadic phenomena, and a different direction of the geoeffective B_z component is apparently explained by a different configuration of neutral lines in AR 10484 (10501). The latter assumption should be confirmed by the data on the variation in the photospheric field zero line in AR during the solar rotation.

Table 4. Characteristics of shock fronts during three solar–terrestrial storms with AR 10484 (10501). (D) velocity; (φ_N and θ_N) angles of the normals; (υ) the angle between the normal and IMF vector before the front; (B_m and B_{me}) the theoretical (with respect to front characteristics) and experimental values of the magnetic field at the magnetic cloud leading boundary

Date	UT	D, km/s	φ_N, deg.	θ_N, deg.	υ, deg.	B_m	B_{me}
October 24	1448	650	177	–2	45	30	32
November 20	0726	780	176	–7	50	52	56
November 22	1001	475	140	–5	25	6	9

The scenario described above is apparently one of the typical mechanisms of generation of strong solar–terrestrial storms with large B_m in magnetic clouds and, correspondingly, with large planetary indices of geomagnetic activity. During the storm of November 22, 2003, the near-Earth satellites were south of AR 10501 and HCS in the high-speed rarefied stream from the coronal hole (Fig. 12) far from the rigid wall (HCS). Moreover, subsector boundaries were absent near the satellites (Fig. 1 in [Ivanov et al., 2005]); therefore, sporadic ejections from AR 10501 after the flares of November 19–20, 2003 (Table 3) propagated in the interplanetary medium with a low counterpressure. The bow shock after the most powerful sf 2b flare, which occurred at 0738 UT on November 20, was responsible for only a weak dynamic impact on the magnetic cloud. The B_m value in the cloud determined from the formula $B_m = (8\pi n_{pn} n_1)^{1/2}(D - V_{N1})$ [Ivanov et al., 1974] was so small (Table 4) that the cloud was hardly discernible in this disturbance and was distinguished conditionally (Fig. 11) based on the variations in the IMF components and on the identical directions of the axes of this cloud and the cloud observed on November 20.

Since any solar–terrestrial storm represents the chain of complicated phenomena, many various data should be used to analyze such a storm. The development of experimental studies of the Sun and interplanetary medium gradually eliminates the historical deficit of these data, and data availability via the Internet within the scope of international programs on solar–terrestrial physics creates prerequisites for constructing scenarios of storms, especially of such storms the intensity of which and the effect on the near-Earth space are extreme. Although the main efforts are as before bend to profoundly studying specific and local manifestations of these storms, the first steps have been recently made toward the phenomenological ordering of the entire complex of individual storm phenomena from the Sun to the Earth and toward the development on this basis of more or less specific and logical scenarios of the physical processes responsible for several solar–terrestrial storms that occurred on January 6–10, 1997 [Ivanov et al., 2004]; on May 12–15, 1997 [Ivanov et al., 2004a]; on July 15, 2000 [Manoharan et al., 2001; Ivanov et al., 2005a]; in late October–early November, 2003 [Veselovsky et al., 2004; Eselevich and Eselevich, 2004; Ivanov et al., 2005; Wang et al., 2005]; on November 18–20, 2003 [Yermolaev et al., 2005]; and in November 2004 [Yermolaev et al., 2005a]. The opposite processes of global MHD modeling of individual storms also took place. The storms observed on January 6–10, 1997 [Wu et al., 1999]; May 12–15, 1999 [Webb et al., 2000 [Webb et al., 2000; Odstrcil et al., 2004, 2005]; and July 15, 2000 [Dryer et al., 2001] were simulated.

11. CONCLUSIONS

(1) The solar–terrestrial storm of November 18–20, 2003, belong to the class of complex flare–hole–filamentary–streamer storms according to the classification of storms with respect to their solar sources [Ivanov, 1996, 1998]. This storm originated in the main zone of active longitudes dominating in the current cycle. The corresponding near-Earth MHD disturbance was observed on HCS and in the closest proximity to this sheet.

(2) The complicated bow shock layer behind the quasiparallel shock, wide boundary layer at a transition from the shock to the magnetic cloud with the antiparallel (reconnecting) IMF B_z components and high-speed flow along the cloud boundary, and magnetic cloud composed of the magnetic cavity and hot plasma (filament substance) enriched in helium and packed into the cavity were identified in the structure of the near-Earth MHD disturbance.

(3) It was noted that the axes of symmetry of the active filament, transient coronal hole, coronal mass ejection, and zero line of the large-scale solar magnetic field (HCS), as well as the axis of the near-Earth magnetic cloud, were parallel. A similar parallelism was previously detected for the solar–terrestrial storm of July 15, 2000 [Ivanov et al., 2005a] and corresponds to the conclusions on a three-dimensional configuration of CMEs based on results of the statistical studies [Cremades and Bothmer, 2004].

(4) A comparison of the near-Earth MHD disturbances during three storms after flares from the same AR 10484 (10501) indicated that strong MHD disturbances with a good reproducibility of the velocity field behind quasiparallel shocks were observed when the Earth was identically located west of AR and HCS (storms of October 24 and November 20, 2003, on HCS); MHD disturbances were weak when the Earth

was located east of AR and HCS (storm of November 21–22 in the coronal hole).

(5) Strong disturbances on HCS observed on November 20 and 24, specifically, large B_{max} values in magnetic clouds and proton temperature rise in the cloud of November 20, were caused by an increase in pressure behind reflected shocks originated during the interaction between HCS and shocks caused by sporadic phenomena in AR 10484 (10501).

(6) In all cases the magnetic field in the clouds satisfied the formula $B_{max} = (8\pi m_p n_1)^{1/2}(D - \mathbf{V}_1\mathbf{N})$ obtained from the condition of equality of the magnetic pressure at the leading cloud boundary and the dynamic impact on the cloud [Ivanov et al., 1974].

ACKNOWLEDGMENTS

We are grateful to N.F. Ness, D.J. McComas, S. Kokubun, and the CDAWeb group for data on IMF, the solar wind and Geotail satellite trajectories, as well as to A.I. Zavoikina for the help in preparing the paper.

This work was supported by the Russian Foundation for Basic Research (project no. 03-02-16340); INTAS (grant 03-51-6206); and Fundamental Research Program, Department of Physical Sciences, Russian Academy of Sciences (state contract 1002-251/OFN-16/041-05/10603-630).

REFERENCES

1. H. Cremades and V. Bothmer, "On the Three-Dimensional Configuration of Coronal Mass Ejections," Astron. Astrophys., No. 422, 307–322 (2004).
2. M. Dryer, C. D. Fry, W. Sun, et al., "Propagation in Real Time of the July 14 Heliospheric Shock Wave and Its Companions during the "Bastille" Epoch," Sol. Phys. **20** (1/2), 267–286 (2001).
3. V. G. Eselevich and M. V. Eselevich, "Sporadic Plasma Flows and Their Sources during Extreme Solar Activity from October 26 to November 6, 2003," Kosm. Issled. **42** (6), 595–607 (2004).
4. J. T. Gosling, M. F. Thomson, S. J. Bame, et al., "The Eastward Deflection of Coronal Mass Ejecta in Interplanetary Space," J. Geophys. Res. **92A**, 12399–12406 (1987).
5. K. G. Ivanov and A. F. Kharshiladze, "The Series of Solar–Terrestrial Superstorms of May–October 2000: 1. Structure and Dynamics of the Open Solar Magnetic Field," Geomagn. Aeron. **44** (1), 3–8 (2004) [Geomagn. Aeron. **44**, 1–6 (2004)].
6. K. G. Ivanov, "Head-on Collision of Symmetric Shocks in Magnetic Hydrodynamics," Pis'ma Zh. Tekh. Fiz. **7** (10), 595–598 (1981a).
7. K. G. Ivanov, "On a Strong Suppression of Interplanetary Shocks during their Interaction in Complex Flows Caused by Flare Series," Geomagn. Aeron. **21** (4), 750–752 (1981).
8. K. G. Ivanov, "The Series of Solar–Terrestrial Superstorms of May–October 2000: 2. Open Magnetic Field and Sunspots," Geomagn. Aeron. **44** (2), 147–154 (2004b) [Geomagn. Aeron. **44**, 131–138 (2004b)].
9. K. G. Ivanov, "The Series of Solar–Terrestrial Superstorms of May–October 2000: 3. Sporadic Phenomena in AR 9077 and Their Relation to the Large-Scale Open Magnetic Field," Geomagn. Aeron. **44** (5), 590–596 (2004a) [Geomagn. Aeron. **44**, 543–550 (2004a)].
10. K. G. Ivanov, "Solar Sources of Interplanetary Plasma Streams at the Earth's Orbit," Int. J. Geomagn. Aeron **1** (1), 1–8 (1998).
11. K. G. Ivanov, "Solar Sources of the Interplanetary Plasma Streams in the Earth's Orbit," Geomagn. Aeron. **36** (2), 19–27 (1996) [Geomagn. Aeron. **36**, 158–164 (1996)].
12. K. G. Ivanov, "Specification of the Phenomenological Model of the Interplanetary Flare Stream: Slow Wave and Boundary Layer," Geomagn. Aeron. **21** (1), 22–25 (1984).
13. K. G. Ivanov, A. F. Kharshiladze, E. P. Romashets, et al., "Slow Dynamics of Photospheric Regions of the Open Magnetic Field of the Sun, Solar Activity Phenomena, Substructure of the Interplanetary Medium and Near-Earth Disturbances of the Early 23 Rd Cycle: December 1996 - February 1997 Events," Int. J. Geomagn. Aeron. **4** (3), 175–194 (2003b).
14. K. G. Ivanov, A. F. Kharshiladze, and E. P. Romashets, "Solar–Terrestrial Storms of October 2003. 1. Solar Sources and Near-Earth Interplanetary Disturbances," Geomagn. Aeron. **45** (1), 5–22 (2005) [Geomagn. Aeron. **45**, 3–19 (2005b)].
15. K. G. Ivanov, A. V. Belov, A. F. Kharshiladze, et al., "Slow Dynamics … March–June 1997 Events," Int. J. Geomagn. Aeron. **4** (2), 91–109 (2003a).
16. K. G. Ivanov, E. P. Romashets, and M. Vandas, "The Series of Solar–Terrestrial Extra Storms of May–October 2000. 4. Structure of the Bow Shock Layer and Configuration of the Near-Earth Magnetic Cloud on July 15," Geomagn. Aeron. **45** (3) 336–346 (2005a) [Geomagn. Aeron. **45**, 315–325 (2005a)].
17. K. G. Ivanov, N. V. Mikerina, and L. V. Evdokimova, "Typical Series of Strong Discontinuities in the Leading Part of the Nonstationary Flow of Interplanetary Plasma," Geomagn. Aeron. **14** (5), 777–783 (1974).
18. J. Krall, J. Chen, R. T. Duffin, et al., "Erupting Solar Magnetic Flux Ropes: Theory and Observation," Astrophys. J. **562** (2), 1045–1057 (2001).
19. P. K. Manoharan, M. Tokumaru, M. Pic, et al., "Coronal Mass Ejection of 2000 July Flare Event / Imaging from Near-Sun to Earth Environment," Astrophys. J. **559** (2), 1180–1189 (2001).
20. D. Odstrcil, P. Riley, and X. P. Zhao, "Numerical Simulation of the 12 May 1997 Interplanetary CME Event," J. Geophys. Res. **109A** (2004).
21. D. Odstrcil, V. J. Pizzo, and C. N. Arge, "Propagation of the 12 May 1997 Interplanetary CME in Evolving Solar Wind Structures," J. Geophys. Res. **110** (in press).
22. J. R. Spreiter and A. Y. Alksne, "Plasma Flow around the Magnetosphere," Rev. Geophys. **7** (1/2), 11–50 (1969).
23. N. L. Tsintsadze and Ts. D. Loladze, "Interaction between Shocks in Magnetic Hydrodynamics," Zh. Tekh. Fiz. **33** (10), 1206–1209.

24. I. S. Veselovsky et al., "Solar and Heliospheric Phenomena in October–November 2003: Causes and Effects," Kosm. Issled. **42** (5), 453–508 (2004).

25. Y. Wang, P. Ye, G. Zhou, et al., "The Interplanetary Responses to the Great Activities in Late October 2003," Sol. Phys. **226** (2), 337–357 (2005).

26. D. F. Webb, R. P. Lepping, L. F. Burlaga, et al., "The Origin and Development of the May 1997 Magnetic Cloud," J. Geophys. Res. **105**, 27 251–27 259 (2000).

27. S. T. Wu, W. P. Guo, D. J. Michels, and L. F. Burlaga, "MHD Description of the Dynamical Relationships between a Flux Rope Streamer, CME, and Magnetic Cloud: An Analysis of the January 1997 Sun–Earth Connection Event," J. Geophys. Res. **104A**, 14789–14801 (1999).

28. Yu. N. Yermolaev, et al., "A Year Later: Solar, Heliospheric, and Magnetospheric Disturbances in November 2004," Geomagn. Aeron. **45** (6) (2005) [Geomagn. Aeron. **45**, 681–719 (2005).

29. Yu. N. Yermolaev, et al., "Solar and Heliospheric Disturbances that Resulted in the Strongest Storm of November 20, 2003," Geomagn. Aeron. **45** (1), 23–50 (2005) [Geomagn. Aeron. **45**, 20–46 (2005)].